Far-Field RF-Powered Variable Duty Cycle Wireless Sensor Platform

Erez Falkenstein, *Student Member, IEEE*, Daniel Costinett, *Student Member, IEEE*, Regan Zane, *Senior Member, IEEE*, and Zoya Popovic, *Fellow, IEEE*

***Abstract*—This brief discusses a low-power wireless sensor based on commercial components for sensing and data transmission. The sensor is wirelessly powered from the far field through an integrated single or dual-polarization antenna, rectifier, and power management module. Since the unit is intended for mobile use, the variable available power is monitored, and the duty cycle for wireless data transmission adaptively adjusted through the use of a low-power microcontroller and a custom power management circuit. In sleep mode, the circuit consumes 1 μA at 2.5 V.**

***Index Terms*—Power management, radio frequency (RF), rectifier, wireless powering, wireless sensors.**

I. Background and Introduction

MANY electronic devices operate in conditions where it is costly, inconvenient, or impossible to replace a battery or deliver wired power. Some examples include sensors for health monitoring of patients [1], [2], aircraft structural monitoring [3], [4], sensors in hazardous environments, sensors for covert operations, etc. This brief focuses on improving efficiency of delivering power wirelessly to a low-power wireless sensor platform with an electrically small antenna, at most one wavelength on the side. "Low power" in this brief refers to less than 200 μW/cm^2 of incident power density of an electromagnetic wave in the radio-frequency (RF) range of the spectrum [5]. We specifically consider frequencies that are either in unlicensed industrial–science–medical (ISM) bands, such as 2.45 and 5.8 GHz, or frequencies where power is radiated for other applications and can be potentially scavenged, e.g., the 2-GHz cellular band.

Previous work in this field ranges from very high power values, e.g., powering a helicopter for up to 10 h of flight with a high-power microwave beam [6] to reception of very low radio-wave power densities in the 5-μW/cm^2 range with large aperture antennas [7]. These and other related applications, e.g., [8]–[10], were aimed at directive power beaming where a narrow-beam antenna transmits power in a well-defined direction toward the power receiving device. The antenna arrays deliver power to a single rectifier, whereas in the work presented here, there is one rectifier per antenna element.

Manuscript received May 4, 2011; revised July 26, 2011 and September 26, 2011; accepted October 21, 2011. Date of publication November 22, 2011; date of current version December 14, 2011. This work was supported in part by the Rehabilitation Engineering Research Center for the Advancement of Cognitive Technologies and in part by the Colorado Power Electronics Center. This paper was recommended by Associate Editor G. A. Rincon-Mora.

The authors are with the Department of Electrical, Computer, and Energy Engineering, University of Colorado at Boulder, Boulder, CO 80309 USA (e-mail: zoya@colorado.edu).

Color versions of one or more of the figures in this brief are available online at http://ieeexplore.ieee.org.

Digital Object Identifier 10.1109/TCSII.2011.2173964

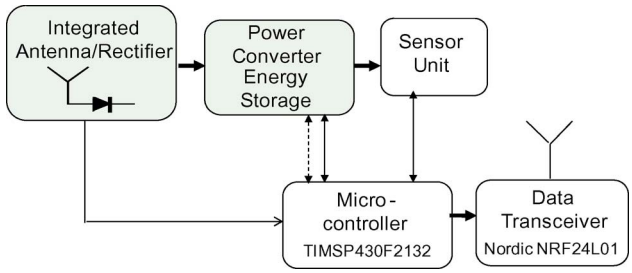

Fig. 1. Block diagram of the far-field RF-powered wireless sensor. The available energy stored is monitored (shown in dashed lines) allowing for adaptive adjustment of the data transmission duty cycle. The low-power microcontroller provides control to the power management circuit, wireless transceiver, and sensor. Power is collected in the far field of one or more ISM transmitters independently of data transmission.

Far-field powering implies plane-wave propagation between antennas at longer range, can be done without line of sight, and is less sensitive to the orientation and position relative to the transmitting antenna. Few applications have taken advantage of this technology for harvesting energy at submilliwatt power levels attributed to the challenges associated with optimizing the interface between the power reception device and typical low-power sensor loads to achieve high overall efficiency. The work in this brief addresses a method for improved far-field powering efficiency at low incident power densities by the integrated design of the power reception device and the power management circuit. It differs from RF identification devices in that powering is independent of signal transmission and is done at different time scales, power levels, and frequencies.

A block diagram for the prototype described in this brief is shown in Fig. 1. An antenna integrated with a rectifier (referred to as a "rectenna" in the literature) receives arbitrarily polarized radiation at one or more of the chosen frequencies at levels below 200 μW/cm^2. The dc output is managed by a digitally controlled power converter in such a way that it always presents close to an optimal dc load to the energy storage device, which provides power to the microcontroller, sensor, and data transceiver. The sensor data are input to a commercial low-power wireless transceiver operating in the 2.4-GHz ISM band. Data transmission is the most power-consuming task and is not continuously done, which is acceptable for most applications. If there is not enough stored energy, the data cannot be transmitted and there is a danger of damaging the storage device. Therefore, the available rectified RF power and the available energy stored are monitored in a closed-loop system allowing for adaptive adjustment of the data transmission duty cycle.

The design method for optimal integration of the RF power receiving circuit and the power management and wireless

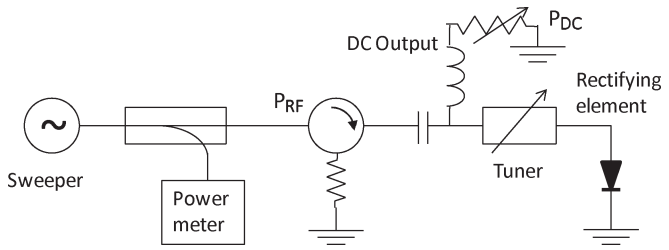

Fig. 2. Modified load-pull measurement setup for characterizing the RF impedance and rectification efficiency of an RF rectifier.

transceiver circuits follows a series of steps in a specific order.

1) The nonlinear modeling of the rectifier for varying dc load over incident RF power levels of interest is performed, experimentally and/or in simulation.
2) The dc power collection circuit is designed to present high impedance to the powering RF signal.
3) The antenna complex impedance is next designed to match the optimal rectifier impedance.
4) After the rectifier is integrated with the passives, careful rectenna characterization for rectified power $P_{\rm DC}$ versus dc load R_L and RF power incident power density $S_{\rm RF}$ is performed. This results in a rectenna Thevenin equivalent.
5) The dc power management circuit is subsequently designed from these data and used to power the sensor(s) and the wireless data transceiver.

In the remainder of this brief, the power receiving integrated antenna/rectifier is discussed, followed by a discussion of the power management circuit and concluding with measured power consumption of the entire wireless sensor platform.

II. RF Power Reception

A plane-wave incident from a transmitter in the far field is used to deliver power remotely to the sensor. The relevant input quantity is power density $S_{\rm RF}$, and the received power at the antenna terminals will be $S_{\rm RF}A_{\rm eff}$, where $A_{\rm eff}$ is the antenna effective area, usually smaller than its geometric area. Therefore, the rectified power available to be delivered to the storage element (battery or capacitor) is

$$P_{\rm DC}(\theta,\phi) = \eta_{\rm RF-DC}(P_{\rm RF}) \cdot A_{\rm eff}(\theta,\phi) \cdot S_{\rm RF}(\theta,\phi)$$

where the rectification efficiency is a function of received RF power due to the nonlinearity of the rectification process. In addition, the above quantities depend on frequency, and the quantity should be integrated over all incidence angles (θ,ϕ).

The highest rectification efficiency is obtained when the diode rectifier is impedance matched to the antenna at the predicted power level since the diode impedance varies with power level. The impedance for optimal rectification is not the same as that for an optimal reflection coefficient and needs to be characterized using nonlinear modeling or measurements. In the method presented here, both a nonlinear model using harmonic balance in Agilent's ADS tool and an experimental model using a load-pull method are performed and compared. The load-pull circuit is a standard characterization method in microwave power amplifier design, and a modified setup for rectifiers is shown in the block diagram in Fig. 2.

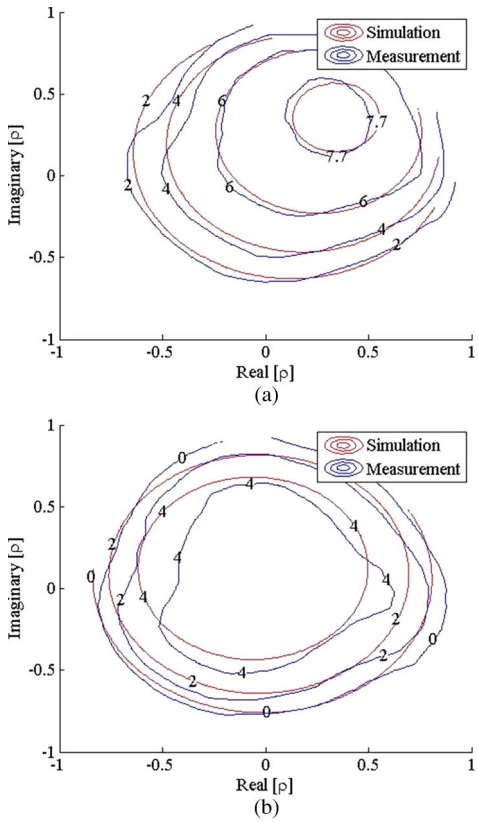

Fig. 3. Measured and simulated constant dc power contours of the real and imaginary parts of the RF reflection coefficient of the diode for (a) $R_L = 460\ \Omega$ and (b) $R_L = 60\ \Omega$. The dc power is expressed in dBm (relative to 1 mW) for an input RF power value of 10 mW.

Varying RF power levels are incident on the rectifier while the RF impedance is changed with the tuner and the dc load impedance varied at a given frequency. For each RF power and dc load, contours of constant rectified dc power are measured as the RF impedance presented to the rectifying element varies from practically a short to an open one. An example of measured data for a Skyworks Schottky SMS-7630-79 diode single-ended rectifier is shown in Fig. 3 for two dc loads and constant input RF power of 0 dBm. The plots show the imaginary and real parts of the reflection coefficient of the diode referenced to a 120-Ω normalization impedance value for plotting convenience and given by:

$$\rho = (Z_{\rm rectifier} - 120)/(Z_{\rm rectifier} + 120).$$

The data in Fig. 3 are useful for optimizing the RF impedance presented to the diode for a given power level for the design of the RF portion of the circuit. However, in order to design the power management circuit that takes the variable rectified power and optimally charges a storage element, the data are plotted, as shown in Fig. 4, which shows that the diode can be reduced to its Thevenin equivalent at dc, provided we keep adjusting the generator impedance to the optimal one for rectification at a given incident power density. This would be sufficient for power management design if the antenna and rectifier integration were 100% efficient but needs to be repeated with the integrated rectenna.

The next step is designing the antenna impedance and the dc collection circuit. A photograph of the back side of a linearly

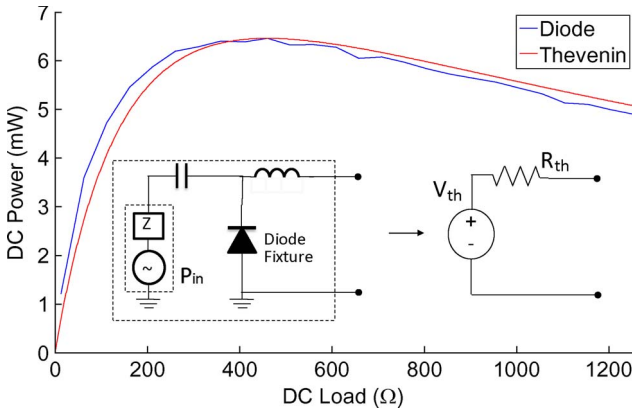

Fig. 4. Load-pull data plotted to form a Thevenin equivalent circuit for the diode rectifier at dc. At each point, the RF impedance is adjusted for optimal rectification, implying that this is the maximum possible rectified power.

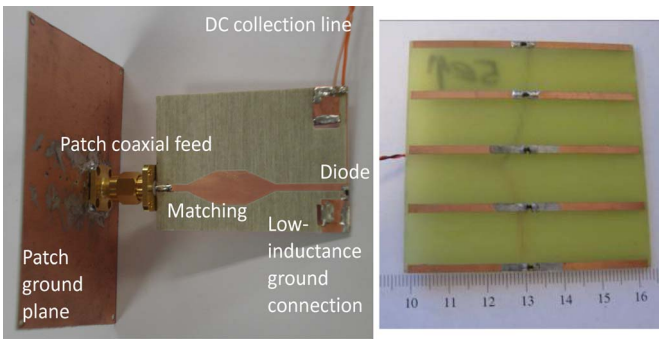

Fig. 5. (Left) Photograph of a 1.96-GHz linearly polarized patch antenna with a diode connected through a microstrip matching circuit. The dc power is taken through an RF-isolated line. The ground plane is 60 mm × 75 mm. (Right) Array of 2.4-GHz dipoles with integrated diodes. The dipole array is omnidirectional in one plane.

polarized patch antenna designed for the 1.96-GHz cell phone band is shown in Fig. 5(a). The antenna and matching circuit is fabricated on a Rogers 4350b 0.762-mm-thick substrate, and the antenna patch dimensions are 38 mm × 39 mm, with a coaxial feed 15-mm offset from the center. A Skyworks Schottky diode is connected to the antenna with a matching circuit. The antenna is simulated using Ansoft HFSS, with good agreement to measured data.

Dual-polarized antennas are also possible, as shown in [10], where each diode rectifies power received in one polarization. In a realistic outdoor multipath environment, polarization is random, thus rectifying two orthogonal polarizations independently, and adding the resulting dc power increases overall efficiency [5]. The patch antenna ground plane results in preferential radiation in the half-space above the ground, but omnidirectional arrays of dipoles such as the one shown in Fig. 5(b) are also possible although not a topic of this brief. The measurements of the integrated rectifier and antenna are performed in an anechoic chamber. The procedure for characterizing the rectenna consists of the following steps.

1) Calibrate power densities at the plane of the rectenna with calibrated antenna of gain G_R

$$S = \frac{P_R 4\pi}{\lambda^2 G_R}. \tag{1}$$

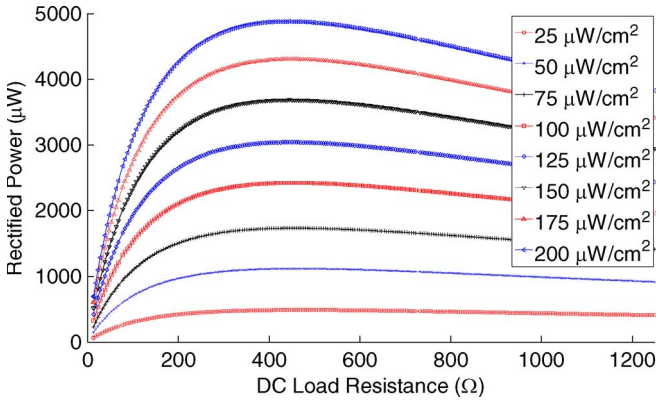

Fig. 6. Example dc power curves for the best performing patch rectenna with various incident power density levels from 25 to 200 μW/cm^2. The load resistance is varied from 0 to 1250 Ω, and the best efficiency occurs for an optimal dc load around 460 Ω in this case.

2) Calculate RF power incident on rectenna, assuming that the effective area is equal to the geometric area of the antenna, which is an overestimate

$$P_{\mathrm{RF}} = S \cdot A_G. \tag{2}$$

3) Measure dc power as a function of dc load resistance.
4) Calculate RF to dc conversion efficiency, which will be an underestimate

$$\eta_{\mathrm{RF-DC}} = \frac{P_{\mathrm{DC}}(R_L)}{P_{\mathrm{RF}}}. \tag{3}$$

Following the above measurement procedure, the integrated rectenna is characterized in terms of its equivalent circuit, similar to the diode case (see Fig. 4). A family of dc curves is shown in Fig. 6 for one example antenna at a specific RF frequency and for various incident power densities. These curves include the antenna efficiency and are the starting points for the power management circuit design, as described below.

When quantifying rectenna efficiency for aperture-type antennas such as a patch, the total input RF power is not easy to quantify from either measurements or simulations in a free-space situation. While the antenna gain, and thus effective area, can be easily found from full-wave electromagnetic simulations, the rectifier loading is not taken into account and the gain is usually calculated for a 50-Ω feed impedance value. Care must be taken when calculating the RF-to-dc conversion efficiency of rectennas since P_{DC} is a function of antenna gain. Fig. 7 illustrates the bounds on efficiency estimation. The highest estimate is obtained when the RF power is estimated from measurement of a passive antenna matched to a 50-Ω feed line, not a rectifier. The lowest efficiency is obtained by the method used in this brief, where the relevant antenna area is assumed to be the geometric area of the antenna [see (2)]. Therefore, the method proposed in this brief gives the conservative efficiency estimate that is useful for system integration, as discussed below.

III. Power Converter Management

As shown in Fig. 1, the power management, sensing, and transmission load are controlled by a single MSP430 microcontroller. In contrast to previous work, the codesign of converter

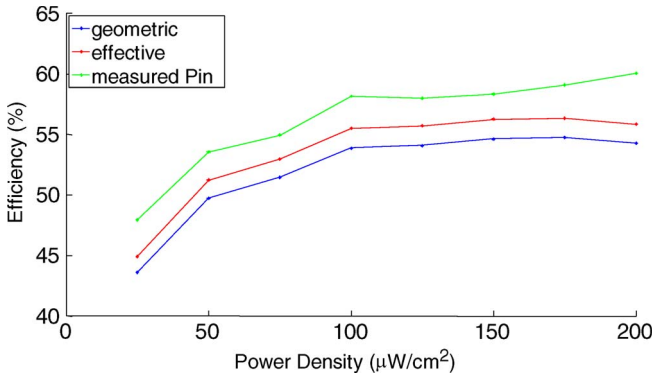

Fig. 7. Estimated RF–dc conversion efficiency of a rectenna as a function of incident power density. The lowest (blue) curve is obtained by the method proposed here. Efficiency values of over 55% are obtained for low incident power densities.

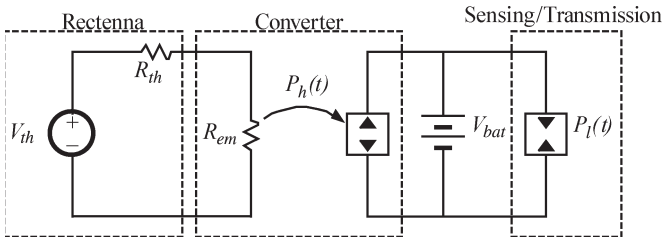

Fig. 8. Averaged model of the converter, rectenna, and load.

and sensing/transmission load, as well as the rectenna and power management, is presented here. This integration allows the microcontroller to dynamically control converter operation to maximize harvested power P_h and to control average load power P_l to match P_l to P_h.

The power flow of the system is shown in Fig. 8. The converter ideally acts as a lossless resistor $R_{\rm em}$ at the input port and transfers input power to the battery at the output port. According to Fig. 6, this operation results in maximum input power P_h from the rectenna if $R_{\rm em}$ of the converter input port is maintained equal to the rectenna optimal dc load, independent of load voltage or power.

The power converter implementation, as shown in Fig. 9, is an asynchronous discontinuous-conduction mode (DCM) boost converter, whose output is a Seiko MS412FE battery with a nominal voltage of 2.5 V. The battery decouples the converter from the load by storing or providing any energy resulting from a temporary mismatch between P_l and P_h. The converter is controlled by the MSP430 microcontroller through a gate drive signal that has both a high-frequency period and duty cycle, i.e., $T_{\rm HF}$ and D, respectively, and a low-frequency period and duty cycle, i.e., $T_{\rm LF}$ and k, respectively, which are altered in order to extract the maximum power from the rectenna.

When operated in DCM, as is guaranteed at the low power levels present in this application, the boost converter input port has the desired resistive average behavior with value

$$R_{\rm em} = 4L/(DT_{\rm HF}k)$$

which is valid under the assumption that $V_{\rm bat} \gg V_{\rm in}$ [1]. This averaging is valid for frequencies well below $T_{\rm LF}$, and it assumes input capacitance $C_{\rm in}$ large enough to maintain negligible voltage ripple across one low-frequency period. Important waveforms of converter operation are shown in Fig. 10. High-

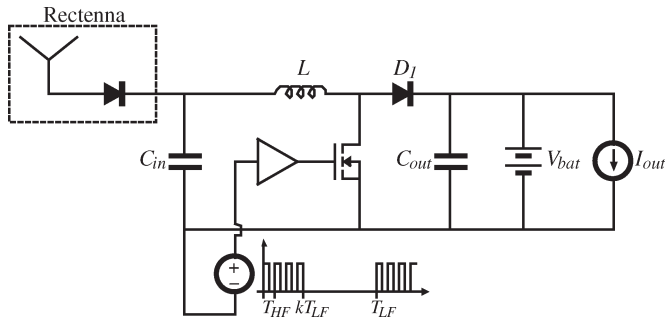

Fig. 9. Circuit diagram of the converter portion of the power management module. $I_{\rm out}$ represents the load on the battery presented by the control, sensing, and transmission circuitry.

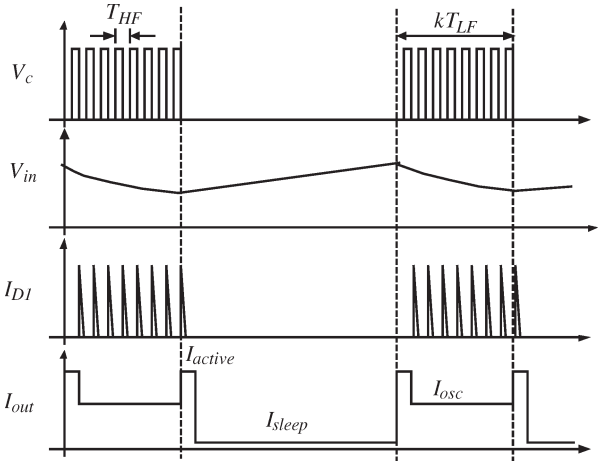

Fig. 10. MOSFET switching waveform V_c, converter input voltage $V_{\rm in}$ (with exaggerated ripple), diode current I_{D1}, and battery load current $I_{\rm ctl}$ caused by the generation of the gate drive signals.

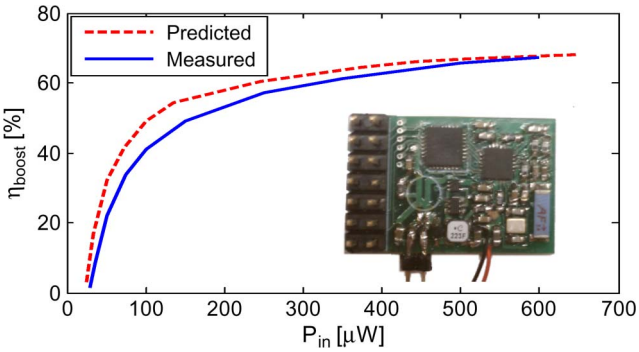

Fig. 11. Measured and predicted efficiency values of the circuit as a function of available input dc power. The 2.1 cm × 1.7 cm circuit contains both power management and sensor/transmitter circuitry.

frequency period $T_{\rm HF}$ is chosen based on a tradeoff between increased control oscillator current $I_{\rm osc}$ required at high frequencies and reduced converter efficiency due to the discharge of $C_{\rm in}$ during $kT_{\rm LF}$. Inductance is optimized offline, based on a sweep of all possible timing parameters and estimated losses in the converter, with the results of the sweep and measured efficiency values shown in Fig. 11 for a 100-μH inductor.

An estimated loss budget for the circuit is given in Fig. 12. Note that, compared to previous circuits, e.g., [1] and [10], this implementation has increased control losses due to the use

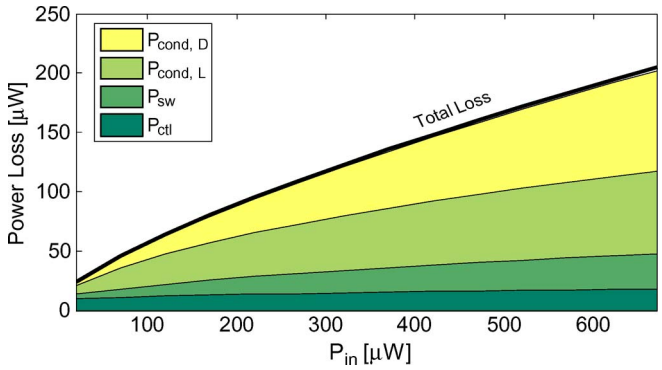

Fig. 12. Loss budget of boost converter circuitry, including control losses, load management, switching losses, inductor ESR, and diode conduction losses. Transistor conduction losses are not significant.

of a microcontroller. However, in previous demonstrations, a microcontroller was a part of the sensing/transmission load, which was not integrated and thus not included in loss calculations. Significant conduction losses in the inductor are also present due to its small size and relatively high equivalent series resistance (ESR). The resulting circuit has higher integration, with a single MSP430 microcontroller controlling the converter, sensing, and transmission, with board area of about 1/5 the size of that previously demonstrated.

IV. Load Management

Referring to Fig. 8, the goal of the load management control is to match the average power consumed by sensing and transmission of data to the average power harvested from the converter circuit. If the device is not actively sensing or transmitting, the processor is allowed to go into a sleep mode, waking only into an active mode briefly on the rising and falling edges of the low-frequency interval, as shown in Fig. 10. When the device is sensing, however, the processor remains in active mode after the $kT_{\rm LF}$ interval for a period of time long enough to sample input and output voltages, as well as any application-specific sensors, then transmits the data. The average current taken from the 2.5-V battery during one sensing and transmission cycle is integrated to obtain the energy per transmission, i.e., $W_{\rm trans} = 20.5\ \mu$J, as shown in [10].

Because the input port acts as a known resistance $R_{\rm em}$, input voltage sensing is sufficient to allow estimation of input power, and transmission period $T_{\rm sense}$ is set to match the power consumed during transmission to the harvested power

$$P_h = \eta_{\rm boost}\left(V_{\rm in}^2/R_{\rm em}\right) \approx W_{\rm trans}/T_{\rm sense} = P_l.$$

To account for the mismatch between P_l and P_h, a battery monitoring routine checks the battery voltage to determine the state of charge and can enable/disable both transmission and converter operation if the battery is at risk of overcharging or discharging completely. For a battery voltage below 2.2 V (90% discharged), all transmission is disabled. If the measured input power is below 25 μW, the converter is disabled, the controller enters the sleep mode with 2.5-μW power consumption, and the $R_{\rm em}$ load on the rectenna is no longer maintained. For a battery voltage above 2.85 V, the converter is shut down so that no further power is sent to the battery and transmission is allowed to continue at the highest duty cycle until the battery voltage drops below 2.8 V. When the entire circuit is tested in an anechoic chamber as a function of incident power density, the results shown in Table I were measured. The transmission duty cycle adaptively decreases with RF power decrease.

TABLE I
Adaptive Transmission Test Results Using the Patch Antenna in Fig. 4. Negative $I_{\rm bat}$ Indicates Net Power Flow Into the Battery

	V_{batt} [V]	S_{RF} [μW/cm^2]	$V_{rectenna}$ [V]	T_{sense}^{-1} [Hz]	I_{bat} [μA]
Regular operation condition	2.5	150	0.826	5	-63.1
		105	0.697	1.5	-57.2
		50	0.505	1.5	-23.4
		30	0.342	0.4	-10
		12.5	0.182	-	-0.4
Overcharge	3	50	0.801	20	132
Discharge	2	50	0.501	-	-43.5

In summary, this brief has presented a wireless sensor platform powered by low power density radio waves. The power management circuit and rectifier/antenna are codesigned reaching total efficiency values in excess of what has been demonstrated to date for these low power levels. At the low power levels, the limiting factor for efficiency is the low-cost hybrid power management circuit, although IC versions have shown to have much better low-power efficiency values [11]. Combining of the sensing, transmission, and power converter circuits leads to a small-size low-complexity highly integrated application circuit.

References

[1] T. Paing, A. Dolgov, J. Shin, J. Morroni, J. Brannan, R. Zane, and Z. Popovic, "Wirelessly powered wireless sensor platform," in *Proc. Eur. Microw. Conf. Dig.*, Munich, Germany, Oct. 2007, pp. 241–244.

[2] J. Bernhard, K. Hietpas, E. George, D. Kuchima, and H. Reis, "An interdisciplinary effort to develop a wireless embedded sensor system to monitor and assess corrosion in the tendons of prestressed concrete girders," in *Proc. IEEE Top. Conf. Wireless Commun. Technol.*, 2003, pp. 241–243.

[3] C. Walsh, S. Rondineau, M. Jankovic, G. Zhao, and Z. Popovic, "A conformal 10-GHz rectenna for wireless powering of piezoelectric sensor electronics," in *Proc. IEEE IMS Dig.*, Long Beach, CA, Jun. 2005, pp. 143–146.

[4] X. Zhao, T. Qian, G. Mei, C. Kwan, R. Zane, C. Walsh, T. Paing, and Z. Popovic, "Active health monitoring of an aircraft wing with an embedded piezoelectric sensor/actuator network," *Smart Mater. Struct.*, vol. 16, no. 4, pp. 1218–1225, Aug. 2007.

[5] J. A. Hagerty, F. B. Helmbrecht, W. H. McCalpin, R. Zane, and Z. B. Popovic, "Recycling ambient microwave energy with broadband antenna arrays," *IEEE Trans. Microw. Theory Tech.*, vol. 52, no. 3, pp. 1014–1024, Mar. 2004.

[6] W. C. Brown, "The history of power transmission by radio waves," *IEEE Trans. Microw. Theory Tech.*, vol. MTT-32, no. 9, pp. 1230–1242, Sep. 1984.

[7] W. Brown, "An experimental low power density rectenna," in *Proc. IEEE MTT-S Int. Microw. Symp. Dig.*, Jul. 1991, vol. 1, pp. 197–200.

[8] J. O. McSpadden, F. E. Little, M. B. Duke, and A. Ignatiev, "An in-space wireless energy transmission experiment," in *Proc. IECEC Energy Convers. Eng. Conf.*, Aug. 1996, vol. 1, pp. 468–473.

[9] J. O. McSpadden, R. M. Dickinson, L. Fan, and K. Chang, "Design and experiments of a high-conversion-efficiency 5.8-GHz rectenna," in *Proc. IEEE MTT-S Int. Microw. Symp. Dig.*, 1998, pp. 1161–1164.

[10] D. Costinett, E. Falkenstein, R. Zane, and Z. Popovic, "RF powered variable duty cycle wireless sensor," in *Proc. EuMC*, 2010, pp. 41–44.

[11] T. Paing, E. A. Falkenstein, R. Zane, and Z. Popovic, "Custom IC for ultra-low power energy scavenging," *IEEE Trans. Power Electron.*, vol. 26, no. 6, pp. 1620–1626, Jun. 2011.